Carcinogenesis, 2024, **45**, 630–641
https://doi.org/10.1093/carcin/bgae048
Advance access publication 24 July 2024
Original Article

OXFORD

Original Article

Absence of lung tumor promotion with reduced tumor size in mice after inhalation of copper welding fumes

Patti C. Zeidler-Erdely[1,*], Vamsi Kodali[1], Lauryn M. Falcone[2], Robert Mercer[1], Stephen S. Leonard[1], Aleksandr B. Stefaniak[3], Lindsay Grose[1], Rebecca Salmen[1], Taylor Trainor-DeArmitt[1], Lori A. Battelli[1], Walter McKinney[1], Samuel Stone[1], Terence G. Meighan[1], Ella Betler[1], Sherri Friend[1], Kristen R. Hobbie[4], Samantha Service[1], Michael Kashon[1], James M. Antonini[1], Aaron Erdely[1]

[1]Health Effects Laboratory Division, National Institute for Occupational Safety and Health, 1000 Frederick Lane, Morgantown, WV 26508, United States
[2]Department of Dermatology, University of Pittsburgh Medical Center, 3708 Fifth Avenue Suite 500.68, Pittsburgh, PA 15213, United States
[3]Respiratory Health Division, National Institute for Occupational Safety and Health, 1000 Frederick Lane, Morgantown, WV 26508, United States
[4]Pathology Department, Inotiv, P.O. Box 13501, Research Triangle Park, NC 27709, United States

[*]Corresponding author. Health Effects Laboratory Division, National Institute for Occupational Safety and Health, 1000 Frederick Lane, Morgantown, WV 26508, United States. E-mail: paz9@cdc.gov

Abstract

Welding fumes are a Group 1 (carcinogenic to humans) carcinogen as classified by the International Agency for Research on Cancer. The process of welding creates inhalable fumes rich in iron (Fe) that may also contain known carcinogenic metals such as chromium (Cr) and nickel (Ni). Epidemiological evidence has shown that both mild steel (Fe-rich) and stainless steel (Fe-rich + Cr + Ni) welding fume exposure increases lung cancer risk, and experimental animal data support these findings. Copper-nickel (CuNi) welding processes have not been investigated in the context of lung cancer. Cu is intriguing, however, given the role of Cu in carcinogenesis and cancer therapeutics. This study examines the potential for a CuNi fume to induce mechanistic key characteristics of carcinogenesis *in vitro* and to promote lung tumorigenesis, using a two-stage mouse bioassay, *in vivo*. Male A/J mice, initiated with 3-methylcholanthrene (MCA; 10 μg/g), were exposed to CuNi fumes or air by whole-body inhalation for 9 weeks (low deposition-LD and high deposition-HD) and then sacrificed at 30 weeks. In BEAS-2B cells, the CuNi fume-induced micronuclei and caused DNA damage as measured by γ-H2AX. The fume exhibited high reactivity and a dose–response in cytotoxicity and oxidative stress. *In vivo*, MCA/CuNi HD and LD significantly decreased lung tumor size and adenomas. MCA/CuNi HD exposure significantly decreased gross-evaluated tumor number. In summary, the CuNi fume *in vitro* exhibited characteristics of a carcinogen, but *in vivo*, the exposure resulted in smaller tumors, fewer adenomas, less hyperplasia severity, and with HD exposure, less overall lung lesions/tumors.

Received: April 12 2024; revised: July 9 2024; accepted: July 19 2024

Graphical Abstract

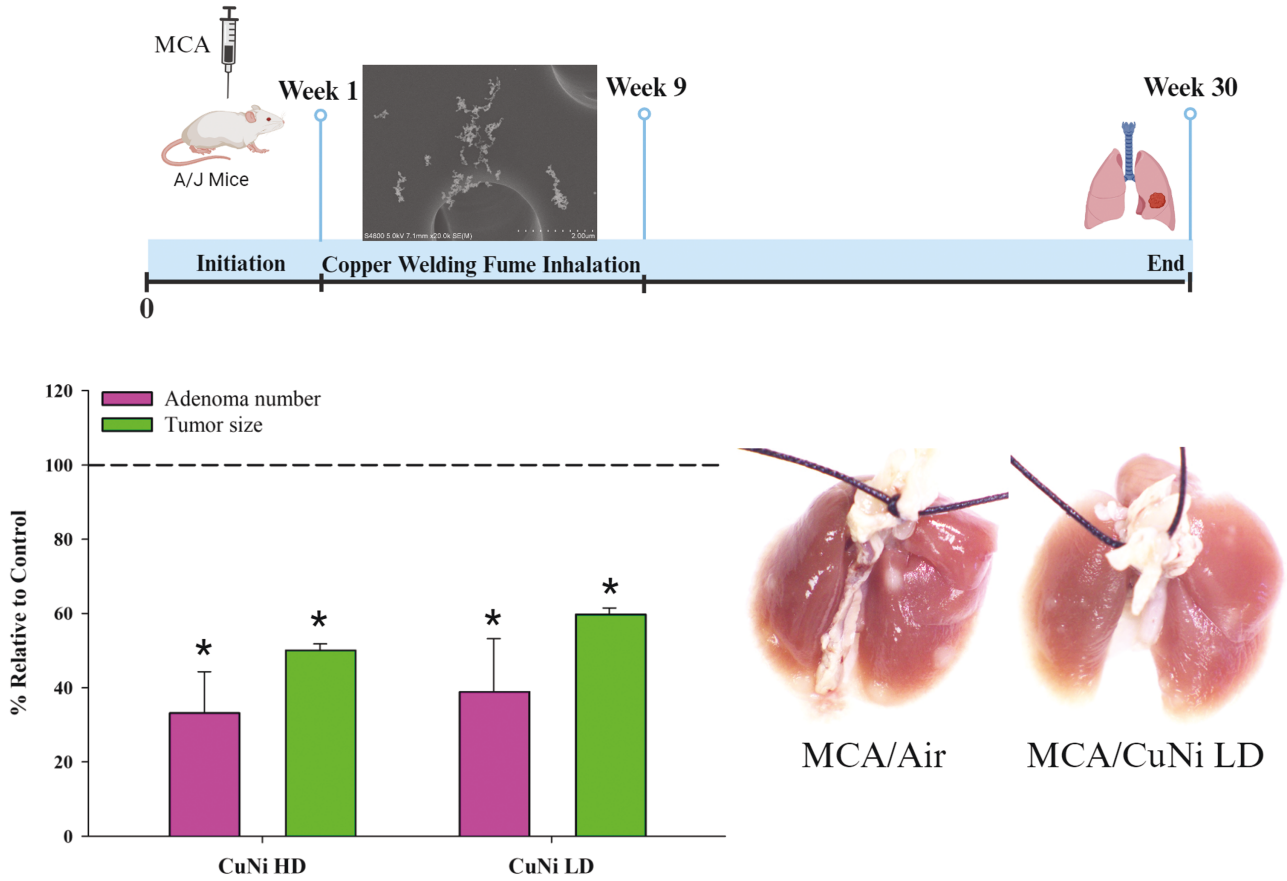

Keywords: metals; two-stage bioassay; inhalation; strain A mouse; lung cancer

Introduction

Welding fumes are a Group 1 (carcinogenic to humans) carcinogen as classified by the International Agency for Research on Cancer. The primary target organ for welding fume-induced cancer is the lung [1]. Welding is a ubiquitous metal-joining process used in many industrial sectors worldwide. The process of welding creates inhalable fumes that are primarily iron (Fe)-rich, as is the case with mild steel (MS) welding. But welding with stainless steel (SS) also creates fumes that contain known carcinogenic metals, including chromium (Cr) and nickel (Ni), in conjunction with the Fe-rich particulate. Epidemiological and experimental animal evidence suggests that both MS (Fe-rich) and SS (Fe-rich + Cr + Ni) welding fumes cause lung cancer [1]. It has been hypothesized that Fe is an important mediator, beyond Cr and Ni, for the known carcinogenic effects of welding fumes [2]. Data from our laboratory provided quantitative evidence to support this hypothesis [3–5].

Welding with copper (Cu) Ni alloys in industrial applications such as marine, power, electrical, and chemical presents a different exposure compared to Cr- and Fe-containing fumes; therefore, the potential adverse health outcomes need to be addressed since the toxicity is relatively unknown [6–9]. Research on Cu-containing welding fumes is warranted given the many roles that Cu serves in normal tissues and in tumors. From a cancer perspective, Cu is especially intriguing because of the emerging therapeutic research involving this metal. For instance, tumor cells are Cu-dependent; thus, restricting Cu has been shown to have beneficial, tumor-inhibiting effects [10, 11]. Conversely, Cu excess is also therapeutically beneficial as high concentrations are toxic to tumor cells [12]. From a human exposure standpoint, Cu is not classified as a carcinogen by IARC or EPA. Cu, particularly nanometer-sized, is known to be toxic *in vitro*, however [12].

A recent study found a Cu-based drug reduced the number and size of nitrosamine, 4-(methylnitrosamino)-1-(3-pyridyl)-1-butanone (NNK)-induced lung tumors in the A/J mouse [13], which suggests the CuNi fume may not promote tumors like other welding fumes. The primary objectives were to evaluate acellular reactivity, screen for selected key characteristics of carcinogenesis *in vitro*, and use a two-stage (initiation-promotion) mouse lung tumor bioassay to evaluate CuNi welding fume.

Materials and methods

Welding fume inhalation exposure system and aerosol characterization

The design and construction of the welding fume aerosol generator were described in [14]. The automated robotic welder continuously generates welding fumes by welding beads onto 6.35 mm thick plates of MS. A 1.143 mm diameter Lincoln Electric Techalloy 413 MIG welding wire was used and all welding parameters were described in detail [7]. Particle mass concentrations within the whole-body animal

exposure chamber were continuously monitored with a Data RAM (DR-40000 Thermo Electron Co; Franklin, MA), and verified with gravimetric determinations daily. Gas generation was continuously monitored and oxygen (O_2) levels were maintained above the Occupational Safety and Health Administration (OSHA) minimal acceptable level. Ozone (O_3), carbon monoxide (CO), and carbon dioxide (CO_2) were below OSHA permissible exposure limits and NIOSH recommended exposure limits (REL). Welding fume was collected gravimetrically onto 47 mm Nucleopore polycarbonate filters (Whatman; Clinton, PA) for field emission scanning electron microscopy (FESEM) to assess particle size and morphology. The particles were imaged using a Hitachi S4800 Field Emission Scanning Electron Microscope (Hitachi; Tokyo, Japan). Hydrodynamic diameter and zeta potential were determined using dynamic light scattering and laser Doppler electrophoresis, respectively, (Zetasizer ZS90, Malvern Instruments; Worcestershire, UK). Specific surface area (m^2/g) was measured using Brunauer Emmet Teller methodology and density was determined based on International Organization for Standardization (ISO) 23145 as described [15].

In vitro screen for key characteristics of carcinogenesis

Human bronchial epithelial cells (BEAS-2B, CRL-3588) obtained from the American Type Culture Collection (Manassas, VA) were cultured between passages 1 and 15 and tested negative for Mycoplasma contamination. Cells were cultured in Dulbecco's modified Eagle medium supplemented with 10% heat-inactivated fetal bovine serum (R&D Systems; Minneapolis, MN) and 1% penicillin Streptomycin (Invitrogen; Carlsbad, CA) to 70% confluency. CuNi fumes were dispersed in cell culture media by preparing aqueous stock suspensions. Cytotoxicity was evaluated using a 10% volume/volume WST-1 cell proliferation reagent (Sigma–Aldrich; St. Louis, MO) as described [15]. Half-maximal inhibitory concentration (IC50) was determined by regression analysis of the experimental dose–response relationship. CytoTox-ONE™ Reagent (Promega; Madison, WI) was used to evaluate the membrane damage as described [15]. Intracellular oxidative stress due to particle exposure was determined using CellROX® Green (Invitrogen; Waltham, MA) as described [15]. A positive control of 100 µM menadione incubated for 2 h was used. Cells were exposed to 0–50 µg/ml for 4 h to determine the oxidative stress dose–response relationship. The time response (0–24 h) was evaluated at a dose of 12.5 µg/ml. Phospho-Histone H2A.X (Ser139) Rabbit mAb (Alexa fluor 488 conjugated) (Cell Signaling; Beverly, MA) was used to evaluate γ-H2AX in cells after 24 h of exposure, as described [15]. The experiment was performed in triplicates and at least 10 000 cells were analyzed/sampled in each group. Cytokinesis-block micronucleus (CBMN) was performed in accordance with OECD TG487 [16]. Cells were exposed to 0–3.2 µg/ml [concentration less than IC70 (3.7 µg/ml)] for 24 h followed by a 24-h treatment with 4 µg/ml of cytochalasin B (Sigma–Aldrich; St. Louis, MO). Confocal Z stacks were obtained and at least 700–1300 binucleated cells were counted from 3 to 4 independent runs. Two independent reviewers evaluated the micronuclei in the binucleated cells and the average count of the reviewers was used for the final count. V_2O_5 at 0.312 µg/ml served as a positive control for genotoxicity. Acellular reactivity was determined using electron paramagnetic resonance (EPR) spin-trapping as described [17].

Animals

Male A/J mice (age 4–5 weeks) were purchased from Jackson Laboratories (Bar Harbor, ME) and housed in an AAALAC International—specific pathogen-free, environmentally-controlled facility. All mice were free of endogenous pathogens including viruses, bacteria, mycoplasmas, and parasites. Mice were housed in groups of two in ventilated cages and provided high-efficiency particulate-filtered air under a controlled light cycle (12 h light/12 h dark) at a standard temperature (22°C–24°C) and 30%–70% relative humidity. Animals were acclimated to the animal facility for 1 week before beginning the experimental protocols (age 5–6 weeks) and allowed access to a conventional diet (6% irradiated NIH-31 Diet, Envigo RMS; Madison, WI) and tap water *ad libitum*.

Experimental protocol for two-stage lung carcinogenesis bioassay in A/J mice

Our 9-week whole-body inhalation protocol in conjunction with the two-stage (initiation-promotion) model using 3-methylcholanthrene (MCA) as the initiator was used in this study [3, 18]. Two separate sets of mice were exposed for the 9-week duration to CuNi welding fume. Animal set one was a high deposition (HD) exposure scenario and 120 mice were weight-matched and randomized into four exposure groups [Corn oil (CO)/Air; CO/CuNi; MCA/Air; MCA/CuNi; n = 30/group]. At week 0, mice were intraperitoneally (IP) injected with MCA (Sigma–Aldrich; St. Louis, MO) dissolved in CO (Sigma–Aldrich; St. Louis, MO) at a dose of 10 µg/g of body weight or CO alone. At week 1 post-initiation, mice were exposed by whole-body inhalation to CuNi welding fume aerosols or filtered air for 4 h/day, 4 days/week, for 9 weeks (35 days total; mean concentration was 32.6 ± 19.0 mg/m^3). Animal set two was a low deposition (LD) scenario and 60 mice were weight-matched and randomized into two exposure groups (MCA/Air and MCA/CuNi; n = 30/group). The CO groups were not repeated in this scenario because CuNi alone was found to have no significant effect on HD exposure. At 1 week post-initiation mice were exposed to CuNi welding fume aerosols or filtered air for 2 h/day, 4 days/week, for 9 weeks (35 days total; mean concentration was 21.0 ± 6.6 mg/m^3).

Throughout the study, mice were weighed biweekly. Mice were euthanized with sodium pentobarbital [100–300 mg/kg IP] (Vortech Pharmaceuticals; Dearborn, MI), weighed, and exsanguinated via the vena cava. All internal organs were examined for the presence of tumors. Then, the whole lung was excised and inflated with 10% neutral buffered formalin. Twenty-four hours post-fixation, lung tumors were counted under a modular stereomicroscope (Leica Microsystems; Morrisville, NC) and measured using digital calipers. Gross lung images were taken using an Olympus DP21 digital camera (Olympus America; San Jose, CA). Lung tumor incidence was recorded as the percentage of tumor-bearing mice in each group. Lung tumor multiplicity for each group was determined as the average tumor number per mouse lung including mice with no tumors as described previously [3, 18–21].

Histopathological analysis of CuNi fume-exposed lung tissue

Lungs were embedded in paraffin and a 5 µm standardized section was cut and stained with hematoxylin and eosin. Slides were interpreted by a contracted board-certified veterinary pathologist. Neoplastic findings were recorded as present and the number of tumors/section were recorded. The diagnoses of alveolar epithelial hyperplasia and bronchiolo-alveolar adenoma were based upon well-established criteria and classified using standard published International Harmonization of Nomenclature and Diagnostic Criteria for Lesions (INHAND) terminology to the extent possible [22, 23]. In addition, the severity of the hyperplasia was recorded as the severity of the most severe lesion observed. Non-neoplastic histopathologic findings were graded and recorded using the grading scale derived from [24] as follows: No Visible Lesion [(NVL) tissue considered to be normal], 1 = minimal, 2 = mild, 3 = moderate, 4 = marked. All lung sections from animals that survived to 30 weeks were evaluated except for three slides from the MCA/Air group of the HD exposure. Both microscopic and gross-enumerated lung tumor numbers were statistically evaluated for all animals surviving to the 30-week terminal sacrifice.

Enhanced dark-field light microscopy imaging of CuNi fume-exposed HD lung tissue

Welding fume particles in sections from exposed lungs were assessed using an enhanced dark-field optical system. Welding fume particles scatter light significantly greater than the surrounding tissues due to a difference in refractive index, nanometer size, and the crystalline structure of the particles. The enhanced dark-field optical system images light scattered in the section and, thus, particles in the section stand out from the surrounding tissues with high contrast [25–28]. Sections for dark-field examination were cut from paraffin blocks at 5 µm thickness and collected on ultrasonically cleaned, laser-cut slides (Schott North America; Elmsford, NY). After staining with Sirius Red-Hematoxylin, slides were dehydrated in xylene and coverslipped with Permount (Fisher Scientific Co.; Pittsburgh, PA) containing 5%, by volume xylene. Just before mounting, the xylene-Permount was centrifuged (10 000×*g* for 10 min) to remove contaminating particles. The optical microscopes consist of a transmitted light microscope (Olympus B63 with motorized condenser, controller, and reflected light system) and a CytoViva EDM (CytoViva; Auburn, AL). Both were equipped with an Olympus DP73 digital camera with cellsens Dimension camera control and measurement software (Olympus America; Center Valley, PA). Images for both systems were taken at either high resolution 4800 × 3600 pixels or 2400 × 1800 pixels.

Statistical comparisons and analysis

Statistical analyses were performed using either JMP version 13 or SAS version 9.4 for Windows and only utilized data from those animals surviving to the 30-week terminal sacrifice. Body weight data were analyzed using a two-way mixed-model analysis of variance with repeated measures using "Proc Mixed." Variables obtained from *in vitro* studies were analyzed using one- and two-way ANOVAs. Gross tumor counts were analyzed using nonparametric Kruskal–Wallis tests and followed by pair-wise comparisons using the Wilcoxon Rank Sums test. Tumor incidence was analyzed using a Chi-square test in SAS "Proc Freq," while tumor multiplicity was analyzed using Poisson regression in SAS "Proc Genmod." In cases where over-dispersion existed, a negative binomial regression was performed. Analyses were performed independently on CO and MCA-treated animals. For tumor size comparisons between MCA-treated animals, a two-sided *t*-test was performed only on data from animals with tumors. For all analyses, a $P < .05$ was set as the criteria for significance.

Results

Characterization

SEM image of the generated welding fume shows primary particles in the nanometer size range linked together in elongated chain-like structures often with several branches (Fig. 1A). Most of the particles were between 0.1 and 1 µm in diameter, with a mass median aerodynamic diameter of 0.43 µm as reported in [7]. Dynamic light scattering showed that the particle had a hydrodynamic diameter of 132 nm and a zeta potential of—10 mV at physiological pH when dispersed in cell culture media. The polydispersity index indicated wide distribution in the particle's aggregates in cell culture media. CuNi welding fume had a tapped density of 6.25 g/cm^3 and a surface area of 33.07 m^2/g (Fig. 1B). Elemental analysis by inductively coupled plasma atomic emission spectroscopy (ICP-AES) was previously reported in [7] (Fig. 1C). The CuNi fume was 76.3% Cu; 11.6% Ni, and 5.10% Fe by weight percent with the remaining metal content being 2.9% titanium (Ti), 2.3% manganese (Mn), and trace metals. EPR on the CuNi fume produced the typical 1:2:2:1 spectrum, characteristic of hydroxyl radical, showing the fume was reactive (Fig. 1D). CuNi fume produced 1.5-fold higher free radicals than the positive control [2 mM Cr(VI)].

In vitro screen for key characteristics of carcinogenesis

The cytotoxicity potential of CuNi fume was assessed by measuring the cellular ability to reduce the WST-1 reagent. There was a steep dose-dependent increase in toxicity after 24 h of exposure (Fig. 2A). There was a significant change in cytotoxicity from a dose >3.125 µg/ml. The IC50 and IC70 for CuNi fume were found to be 6.6 µg/ml and 3.7 µg/ml, respectively. Membrane damage was evaluated by LDH levels in the supernatant, and only the highest dose caused a significant effect (Fig. 2B). Intracellular reactive oxygen species (ROS) was evaluated as a dose and time response (Fig. 2D). There was a 5-fold increase in ROS after 4 h of exposure with 50 µg/ml. There was a continuous significant change from 16 h with the 12.5 µg/ml exposure. Genotoxicity was evaluated at 0–3.2 µg/ml, doses less than IC70. Phosphorylation of H2AX, a cellular response to repair double-strand DNA breaks was assessed as a complimentary measure to the micronuclei to determine genotoxicity. There was a significant increase in the level of γ-H2AX with 1.8 and 3.2 µg/ml of CuNi fume compared to control cells. Within the doses, there was not a significant alteration in the level of γ-H2AX (Fig. 2C). *In vitro* micronucleus formation was evaluated using CBMN (Fig. 2E). Actin polymerization inhibitor cytochalasin B was used to block cytokinesis after CuNi fume treatment to prevent the separation of daughter cells after

A.

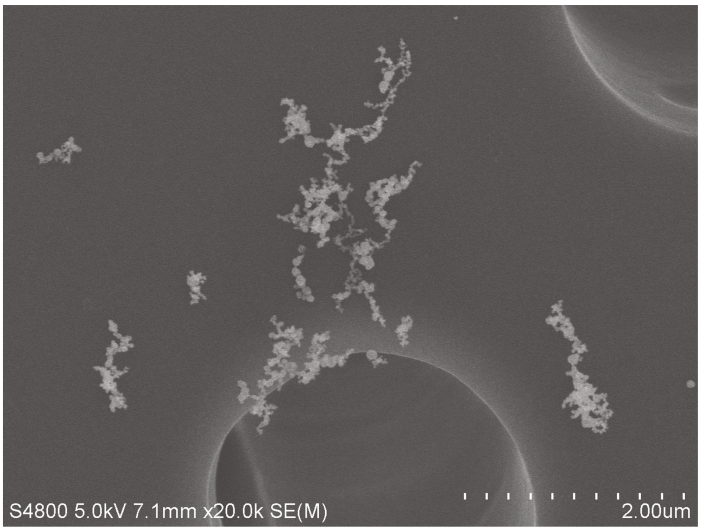

B.

CuNi Fume Characteristics	
Aerodynamic Diameter (MMAD)	0.43 µm (1.48 GSD)
Hydrodynamic Diameter (D_h)	132 ± 7 (nm)
Polydispersity Index (PDI)	0.53 ± 0.03
Zeta Potential (ζ)	-10 ± 0.15 (mV)
Electrophoretic Mobility	- 0.72 ± 0.01 (µmcm/Vs)
Density	6.25 ± 0.10 (g/cm^3)
Surface Area	33.07 ± 0.12 (m^2/g)

C.

Metal Components	% Total CuNi
Cu	76.4
Ni	11.6
Fe	5.1
Other (Ti, Mn)	< 5

D.

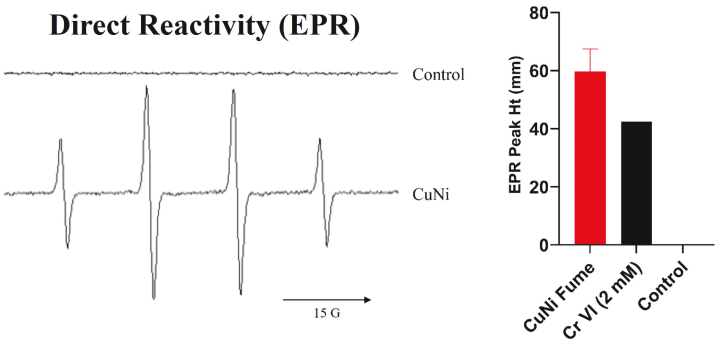

Figure 1 Field emission electron scanning microscope image of CuNi welding fume generated by the automated robotic welder (A). Characterization of generated CuNi welding fume (B). The mass median aerodynamic diameter was reported in [7]. Elemental analysis by inductively coupled plasma atomic emission spectroscopy (ICP-AES) previously reported in [7] (C). EPR on the CuNi welding fume produced the typical 1:2:2:1 spectrum, characteristic for OH, and produced 1.5-fold higher free radicals than the positive control [2 mM Cr(VI)]. The EPR spectrometer settings were: receiver gain 1.00 × 10^4; centerfield 3484 G; field width 100 G; scan time 100 G; power 63.460 mW; frequency 9.760 GHz (D).

mitosis, leading to the formation of binucleate cells. Only the highest dose (3.2 µg/ml) and the positive control cells had significant binucleated cells with MN compared to control cells with no treatment. As seen in the representative confocal images, binucleate cells had no MN, one or multiple MN. To account for the multiple micronuclei, the total MN in the binucleated cells was also evaluated. CuNi fume at the low (0.18 µg/ml) and high (3.2 µg/ml) doses had a significant increase in total MN compared to control cells. Like our observation with γ-H2AX, there was a significant increase in binucleated cells with MN and total MN compared to control cells.

Pulmonary deposition of CuNi welding fume

We have thoroughly described the lung deposition in terms of human relevance for the welding inhalation exposure animal model [7, 29]. We previously quantitated mouse lung deposition by inductively coupled plasma atomic emission spectroscopy and alveolar accumulation was estimated to be 1.28 µg/h with an exposure of 43 mg/m^3 [7]. Proportionally in this study, CuNi HD was 0.97 µg/h for ~136 µg alveolar deposition (32.6 ± 19.0 mg/m^3; 4 h/day for 35 days over 9 weeks), and CuNi LD was 0.63 µg/h for ~44 µg alveolar deposition (21.0 ± 6.6 mg/m^3; 2 h/day for 35 days over 9 weeks). Therefore, the CuNi LD had a lower dose rate as well as one-third of the final deposition over the inhalation exposure time course.

Body weight, morbidity, and mortality

The 9-week whole-body inhalation protocol in conjunction with the two-stage (initiation-promotion) model is shown in Fig. 3A. Exposure to CuNi LD fume caused a significant difference in weight gain at weeks 2 and 4 of the 9-week inhalation exposure compared to air. This was resolved by the end of the exposure and there was no difference between the groups at 30 weeks post-MCA. Analysis of the slopes of the growth curves revealed that the growth rate over time was also not different between the groups with the LD exposure scenario (Fig. 3C). In contrast, analysis of the slopes for the HD exposure showed that both CO/CuNi and MCA/CuNi HD groups exhibited a significant decrease in growth rate over time compared to CO/Air and MCA/Air. This initial decreased weight gain in the CuNi HD fume groups recovered by about week 18 (Fig. 3B).

Morbidity and mortality throughout the experimental protocols were low and no abnormalities, such as other tumor types besides lung, were found at the terminal sacrifice at 30 weeks. In total, one mouse from the LD (MCA/CuNi) and nine mice from the HD protocol (3 CO/Air; 2

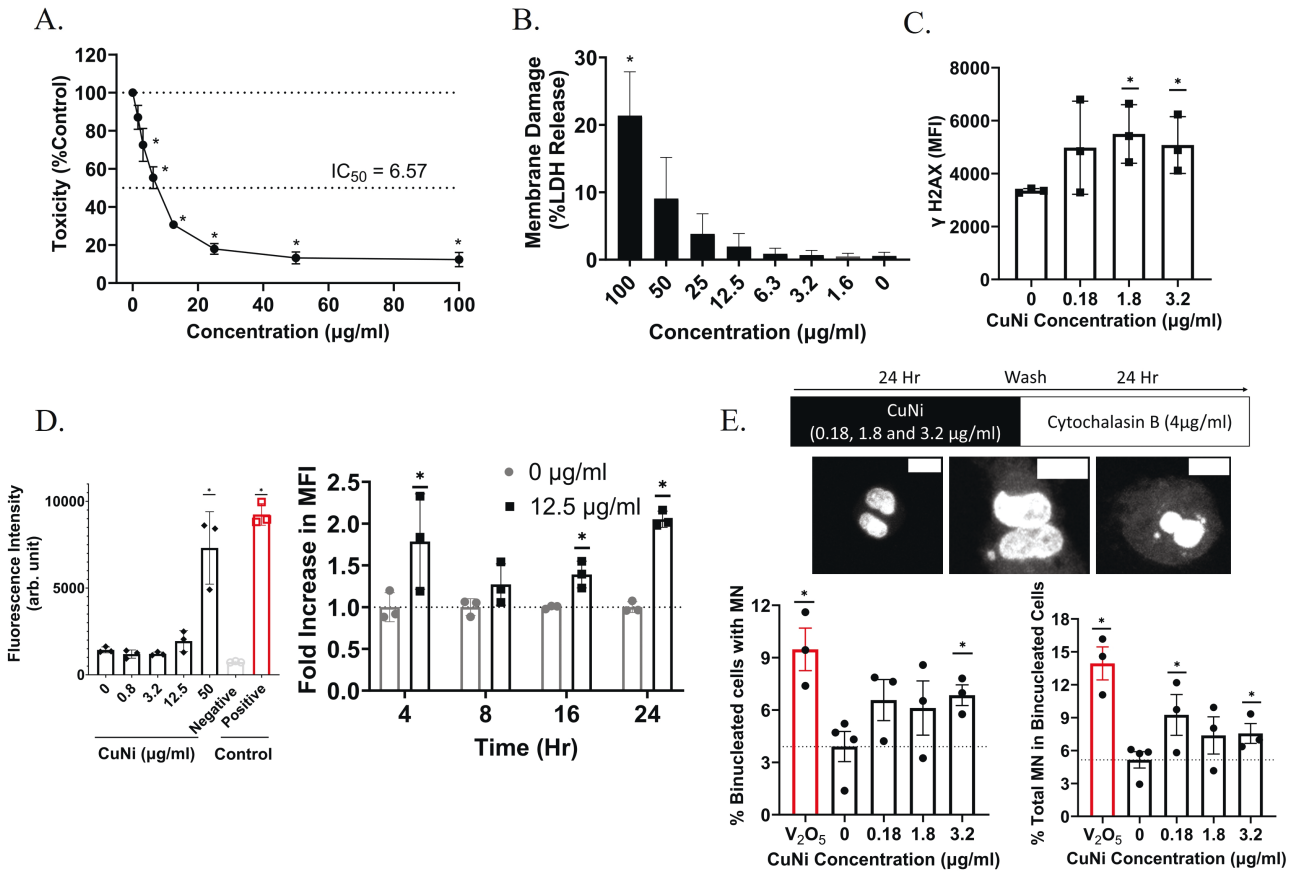

Figure 2 *In vitro* screening of key characteristics of carcinogenesis in human bronchial epithelial cells (BEAS-2B). The cytotoxic potential of CuNi welding fume was assessed by measuring the cellular ability to reduce WST-1 reagent (A). Cell membrane damage was evaluated by LDH levels in the supernatant (B). Phosphorylation of H2AX, a cellular response to repair double-strand DNA breaks (C). Intracellular ROS evaluated as a dose and time response (D). *In vitro* micronucleus formation was evaluated using CBMN and representative confocal images are shown (E; scale bar: 10 µm). *$P < .05$—determination of statistical significance.

MCA/Air; 1 CO/CuNi; 3 MCA/CuNi) were euthanized or died during the course of the study and were not included in the final data analysis. Necropsy determined that all 10 mice had morbidities not associated with the experimental protocol. These included scrotal lesions, head tilts, neck mass, body weight loss, or otherwise 'undetermined' causes.

Two-stage lung carcinogenesis bioassay in A/J mice: gross lung tumor multiplicity and incidence

Gross-enumerated lung tumors in the CuNi LD fume group were not significantly increased compared to air at 30 weeks post-initiation with MCA (Table 1). Tumor multiplicity across all lung lobes increased, but the response was not consistent or significant across the individual lung lobes except for the cardiac. Tumor size was significantly decreased with MCA/CuNi LD fume exposure compared to MCA/Air, 0.70 ± 0.02 versus 1.17 ± 0.04 mm, respectively. CuNi HD fume compared to air exposure did not increase tumor multiplicity in mice initiated with MCA, but, rather, significantly decreased multiplicity at 30 weeks across the individual lung lobes except for the cardiac (Table 1). Similar to the LD group, CuNi HD fume exposure also significantly decreased tumor size (MCA/CuNi, 0.57 ± 0.01 versus MCA/Air, 1.15 ± 0.02 mm). In the CO animals, no significant effect of the CuNi HD welding fume alone on tumor multiplicity was found. The percentage of tumor-bearing mice (tumor incidence) for the LD exposure scenario was 100% in MCA/Air and 97% in MCA/CuNi. In the HD exposure protocol, tumor incidence was CO/Air 22%, CO/CuNi 7%, MCA/Air 100%, and MCA/CuNi 93%. The low tumor incidence in 35- to 36-week-old CO-exposed mice is consistent with previous studies in our lab as well as others [18, 30, 31]. As expected, tumor incidence was high in all MCA-initiated groups (range of 93% to 100%) which confirmed the successful IP administration as well as its carcinogenic effectiveness in A/J mice.

The difference in tumor size caused by CuNi LD and HD welding fume exposure is appreciated in the representative gross images of mouse lung tissue shown in Fig. 4. Gross lung images of a MCA/Air (Fig. 4A) and MCA/CuNi LD welding fume (Fig. 4D) mouse were captured at the 30-week terminal sacrifice. Fixed lung images of a MCA/Air (Fig. 4B) and MCA/CuNi HD fume (Fig. 4E) mouse were captured 24 h after fixation at the terminal sacrifice. Tumors appeared white in color and became more well-defined after fixation which aided in enumeration.

Enhanced dark-field light microscopy imaging of lung tissue

Enhanced dark-field microscopy confirmed the deposition of CuNi welding fume particles in the lungs of exposed animals as the particles scattered light at a much greater intensity than the surrounding lung tissue (Fig. 4F). The lung tissue adjacent to the fume deposits was made visible only by the addition of

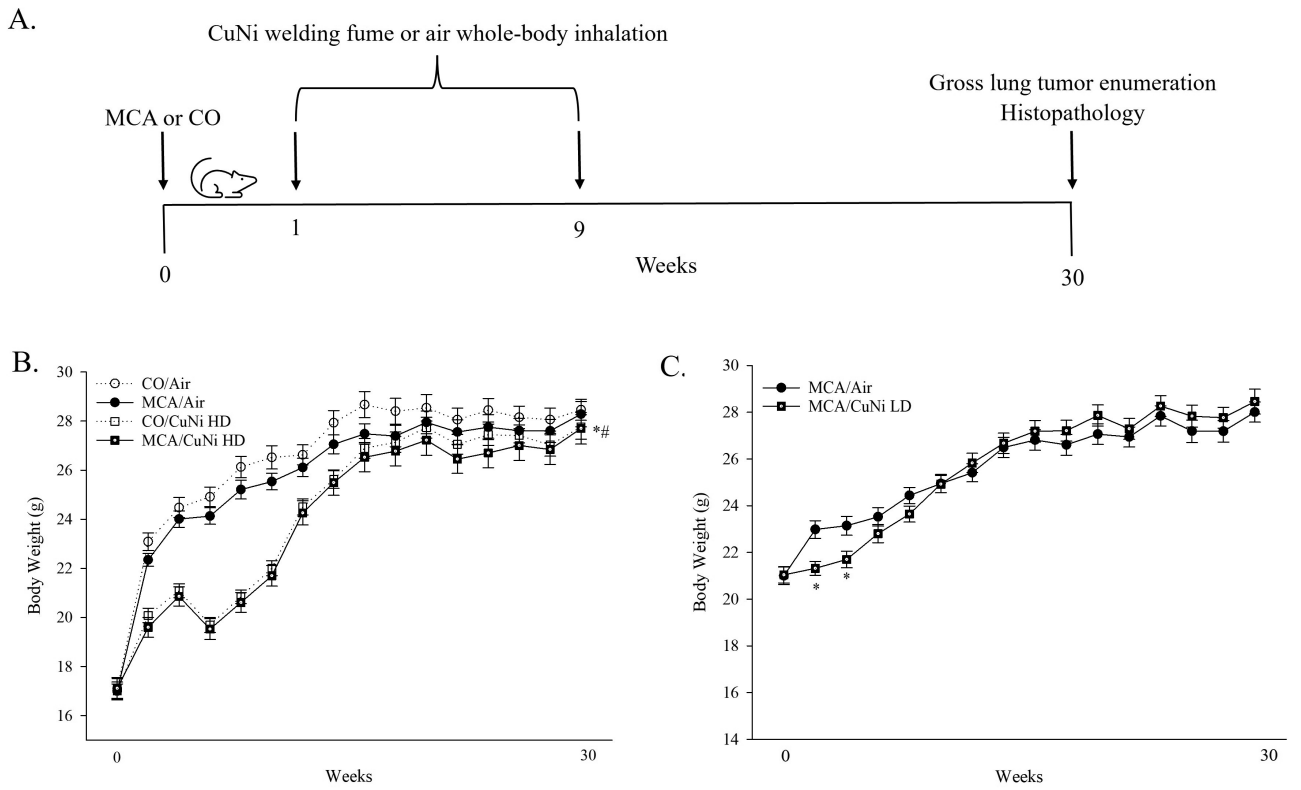

Figure 3 Experimental protocol for two-stage (initiation-promotion) bioassay. HD groups: CO/Air ($n = 30$); CO/CuNi ($n = 30$); MCA/Air ($n = 30$); MCA/CuNi ($n = 30$). LD groups: MCA/Air ($n = 30$) and MCA/CuNi ($n = 30$). Mice were IP injected with MCA (10 μg/g; IP) or CO then 1 week later exposed by whole-body inhalation to CuNi welding fume or air for 2 (LD) or 4 (HD) h/day × 4 day/week × 9 weeks before terminal sacrifice at 30 weeks (A). Body weight changes are presented as mean ± SE. Mice were weighed biweekly (B, HD; C, LD groups) throughout the time course and at the terminal sacrifice. HD—$^{*}P < .05$ for the slope of the growth curve compared to CO/Air and $^{\#}P < .05$ for the slope of the growth curve compared to MCA/Air. LD—$^{*}P < .05$ compared to MCA/Air control at specific time points.

Table 1. Effect of high or low deposition CuNi welding fume on MCA-initiated gross lung tumor numbers, multiplicity, and size across individual mouse lung lobes.

Exposure	*n*	Left	Apical	Cardiac	Diaphragmatic	Azygos	Total	Size (mm)
CO/air	27	4 (0.15 ± 0.07)	0	1 (0.04 ± 0.04)	2 (0.07 ± 0.05)	1 (0.04 ± 0.04)	8 (0.3 ± 0.12)	--
CO/CuNi HD	29	0	0	0	2 (0.07 ± 0.26)	0	2 (0.07 ± 0.05)	--
MCA/air	28	133 (4.75 ± 0.41)	54 (1.93 ± 0.21)	68 (2.43 ± 0.31)	127 (4.54 ± 0.38)	54 (1.93 ± 0.24)	436 (15.6 ± 0.75)	1.15 ± 0.02
MCA/CuNi HD	27	52 (1.93 ± 0.29)*	24 (0.89 ± 0.21)*	51 (1.89 ± 0.32)	38 (1.41 ± 0.28)*	27 (1.00 ± 0.22)*	192 (7.1 ± 0.93)*	0.57 ± 0.01*
MCA/air	30	82 (2.7 ± 0.33)	38 (1.3 ± 0.21)	35 (1.2 ± 0.22)	82 (2.7 ± 0.37)	28 (0.93 ± 0.23)	265 (8.8 ± 0.87)	1.17 ± 0.04
MCA/CuNi LD	29	106 (3.7 ± 0.56)	58 (2.0 ± 0.36)	64 (2.2 ± 0.37)*	88 (3.0 ± 0.45)	43 (1.5 ± 0.32)	359 (12.4 ± 1.5)	0.70 ± 0.02*

CO, corn oil; CuNi, copper-nickel; HD, high deposition; LD, low deposition; MCA, 3-methylcholanthrene. ()—indicate mean ± standard error of the mean number of tumors per individual lobe or lung and includes those with zero tumors; -- indicates not measured.
$^{*}P < 0.05$ compared to corresponding air group.

transmitted light. Welding particle deposits appeared almost exclusively inside macrophages, indicating this fume is phagocytosed by alveolar macrophages. Microscopy images of air-exposed mice showed intact lung tissue and the presence of macrophages devoid of any particulate matter (Fig. 4C).

Two-stage lung carcinogenesis bioassay in A/J mice: histopathological analysis

Severity scores for abnormal morphological findings and numbers of lung lesions observed in lung sections from A/J mice are shown in Fig. 5A–C. Bronchiolo-alveolar adenomas (Fig. 4G) and foci of alveolar epithelial hyperplasia (Fig. 4H) were the most frequent findings and were observed in the lungs of both MCA/Air and MCA/CuNi HD and LD mice. The total number of hyperplastic foci was significantly decreased in the HD group but significantly increased in the MCA/CuNi LD group versus MCA/Air controls. The lesion severity was greater in MCA/Air for both groups, however (Fig. 5A). The total number of adenomas per mouse was significantly decreased in the CuNi HD and LD groups [HD: MCA/Air, 42

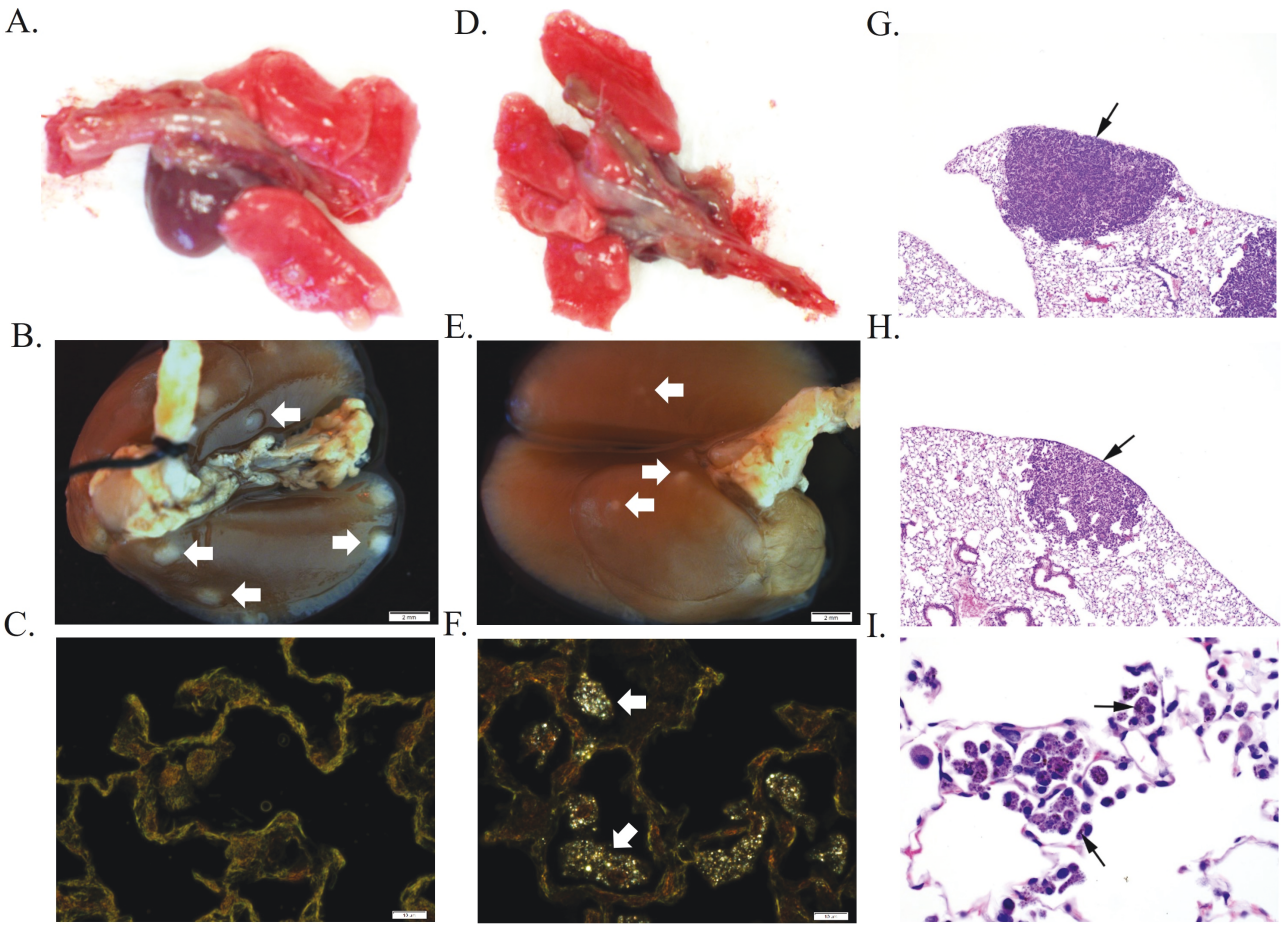

Figure 4 Representative images captured at 30 weeks post-initiation with MCA after 9-week whole-body inhalation exposure. Gross lung images from a MCA/Air (A) and MCA/CuNi LD welding fume-exposed mouse (D). Fixed lung images of tumor (arrows; scale bar: 2 mm) morphology and size from a MCA/Air-exposed (B) and MCA/CuNi HD welding fume-exposed (E) mouse. Enhanced dark-field microscopy image (60×; scale bar: 10 μm) of CuNi welding fume deposits (F, arrows) in the alveoli of a mouse lung. No deposits were present in the alveoli of a mouse lung after filtered air exposure (C). Photomicrographs (4×) of a bronchiolo-alveolar adenoma (G) and an alveolar epithelial hyperplasia (H), moderate, in lung tissue from a MCA/Air-exposed mouse. Photomicrograph (40×) of foreign material within alveolar macrophages (I), mild, in a MCA/CuNi LD-exposed mouse.

(1.7 ± 0.24) versus MCA/CuNi, 15 (0.56 ± 0.19); LD: MCA/Air, 16 (0.53 ± 0.15) versus MCA/CuNi, 6 (0.21 ± 0.08)] (Fig. 5B). Total proliferative lung lesions (adenomas + hyperplasia) were significantly decreased in the HD group [165 (6.6 ± 0.45) versus 102 (3.8 ± 0.55)], but not changed in the LD group [MCA/Air, 94 (3.1 ± 0.38) versus MCA/CuNi, 126 (4.3 ± 0.70)] (Fig. 5C). Maintenance of the normal alveolar structure versus replacement by an abnormal growth pattern differentiated hyperplasia from adenoma, respectively. Foreign material was only observed in the lungs of MCA/CuNi HD and LD mice (Fig. 4I) and was considered a presumptive test article (i.e. CuNi welding fume). Similarly, alveolar neutrophilic inflammation was only observed in MCA/CuNi HD and LD mice. Perivascular lymphocytic infiltrates were observed in the lungs of all MCA/CuNi HD and LD mice and rarely in the MCA/Air groups. Presumably, these lesions in the welding fume-exposed groups were a reactive response to the fume exposure. No other differences in inflammation or repair/injury processes between the groups were observed.

Discussion

CuNi welding fume exhibited significant acellular reactivity and cellular oxidative stress. Cytotoxicity, DNA damage, and micronuclei formation in lung epithelial cells were also found. *In vivo*, inhalation of CuNi fume decreased hyperplasia severity, lung tumor size, overall tumor number with the higher deposited dose, and adenoma formation after initiation with MCA. To our knowledge, this is the first *in vivo* inhalation study investigating the lung tumorigenic potential of a CuNi welding fume; to date, most welding fume-related toxicological research has focused on Fe-rich fumes.

The lack of tumor promotion with CuNi fume contrasts with our previous findings for SS and MS fumes. Both SS (Fe-rich + Cr + Ni) and MS (Fe-rich) welding fumes promoted lung tumorigenesis *in vivo*, which is consistent with epidemiology for an increased lung cancer risk in MS and SS welders [1, 3, 18, 21]. It was subsequently shown that a surrogate Fe component of welding fumes was central to the promoter effect [4]. Also, it is well-documented that SS fumes cause significantly greater pulmonary cytotoxicity and inflammation compared to MS fumes [3, 32–34]. Therefore, the potential for welding fume-induced lung tumorigenesis does not always align with the overall lung toxicity profile. In addition, this study offers further support for Fe as an important mediator for the tumorigenic effect.

Only a few published studies have investigated the pneumotoxicity of Cu-containing fumes. One study found

A.

Effects of high or low deposition CuNi welding fume on MCA-initiated lung lesions in mouse lung sections

Exposure	n	Foreign Material	Perivascular Infiltration Lymphocytic	Neutrophilic Inflammation	Alveolar Epithelial Hyperplasia	Number of Hyperplasia
MCA/Air	25	0 ± 0	0.18 ± 0.08	0 ± 0	3.0 ± 0.18	123 (4.9 ± 0.41)
MCA/CuNi HD	27	1.6 ± 0.11*	1.4 ± 0.10*	0.52 ± 0.09*	1.4 ± 0.15*	87 (3.2 ± 0.48) *
MCA/Air	30	0 ± 0	0.20 ± 0.07	0 ± 0	1.9 ± 0.21	78 (2.6 ± 0.34)
MCA/CuNi LD	29	1.4 ± 0.09*	1.4 ± 0.09*	0.45 ± 0.09*	1.3 ± 0.09*	120 (4.1 ± 0.69)*

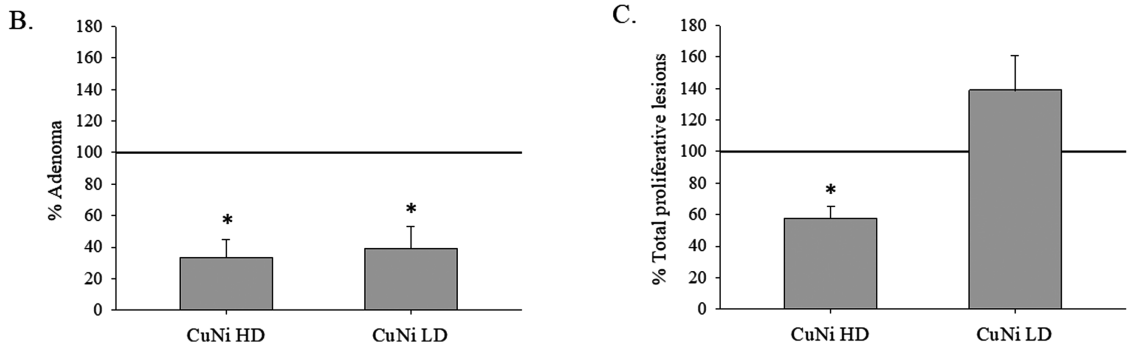

Figure 5 Histopathological severity scores are the averages of the left and right lung lobes and are presented as mean ± standard error of the mean (A). Severity was scored as 1 = minimal, 2 = mild, 3 = moderate, 4 = marked. Hyperplasia data is presented as the total number and parentheses indicate mean ± standard error of the mean number of proliferative lesions per lung and includes mice with zero lesions. Percent of MCA/Air controls adenomas (B) and the total sum of the number of proliferative lesions (adenoma and hyperplasia) for the CuNi HD and LD (C). *$P < .05$—compared to MCA/Air.

that a fume that contained ~6.0% Cu and ~13.4% Ni caused a persistent increase in lung injury and inflammation that was greater than that caused by SS and MS welding fumes [6]. *Ex vivo* mechanistic examination of ROS production and cell viability led the authors to hypothesize that the toxicity of the fume, in comparison, was likely dependent on the direct cytotoxicity of the particles rather than ROS. Further, this same fume *in vitro* resulted in greater cytotoxicity and mitochondrial dysfunction at lower doses than SS or MS fumes [35]. The authors likewise noted that the Cu fume did not induce ROS production but did impair macrophage phagocytosis. Our laboratory investigated the *in vivo* pneumotoxicity associated with short-term (10 days) whole-body inhalation of the CuNi fume tested in the current study. Marked lung cytotoxicity and inflammation, body weight loss, and impaired macrophage phagocytic function were found. These responses resolved progressively, and by 84 days there was no chronic lung pathology except for a small increase in lung macrophage aggregates [7]. Thus, CuNi fume exposure is associated with acute toxicity at levels greater than other well-studied fumes.

While the CuNi fume used in this study has only recently been evaluated, the pulmonary toxicity of Cu compounds, both *in vitro* using lung-associated cells and *in vivo*, has been reported in several studies. *In vitro*, Cu exposure results in dose- and time-dependent increases in cytotoxicity, oxidative stress, cell cycle regulation, and genotoxicity [36–39]. Intracellular release of Cu ions was ascribed as the mechanism of toxicity observed with various forms of Cu [38]. Significant toxicity is associated with nano-sized Cu [38], which is likely applicable to CuNi welding fumes because the generated particles are small chain-like aggregates of nano-sized metals. *In vivo*, Cu inhalation causes pulmonary cytotoxicity, acute inflammation, and impaired host defense against bacterial lung infections [36, 40, 41]. There is significant acute toxicity from Cu exposure (e.g. body weight loss and cytotoxicity), but recovery occurs, and chronic pathology is generally not indicated [42]. Human occupational studies are few, but there is no evidence of lung function decline or chronic inflammation with Cu dust exposure [43]. Our CuNi welding fume results, both *in vitro* and *in vivo*, agreed with these previous findings. *In vitro* CuNi fume-induced cytotoxicity, oxidative stress, and genotoxicity. Further, the CuNi fume, in this study and our previous 10-day inhalation study, resulted in significant lung cytotoxicity and body weight loss, with the HD being more severe. There was a recovery in each instance and no long-term pathology.

The *in vitro* screening of selected key characteristics of carcinogenesis was in line with previous studies with other Cu particulates, although the *in vivo* model resulted in no lung tumor promotion. In research by Stratmann *et al.*, a Cu-containing pigment resulted in a false positive, indicated by acellular and cellular toxicity, that was not duplicated *in vivo*. The authors concluded that the false positive could be due to a lack of clearance *in vitro* in comparison to *in vivo* conditions and other redox homeostatic mechanisms that can adjust for an increased Cu ion load [44]. This would be consistent with the body's ability to tightly regulate Cu. Further, the *in vitro* assays better reflect acute endpoint responses; the two-stage lung bioassay also cautions against using the *in vitro* endpoints (e.g. genotoxicity assessments) to definitively evaluate chronic endpoints.

In addition to the discrepancies between *in vitro* and *in vivo* findings, there appears to be adaptation/resolution with continued Cu exposure *in vivo*. In a recent study by Poland *et al.*, a biphasic response in pulmonary inflammation

was noted despite continued Cu deposition by inhalation. Inflammatory cell influx in the lung peaked during the inhalation regimen and decreased prior to cessation of the 4 weeks of inhalation with the authors noting a biphasic response instead of a monotonic increase over time [42]. That would explain the initial weight loss in our model and in the previous 10-day CuNi fume inhalation study, and recovery even before the exposure ended in the LD group. These studies indicate not only the significant potential for acute toxicity of Cu compounds and the CuNi fume but also adaptation and resolution despite continued exposure *in vivo*.

SS and CuNi fume both induce inflammation, cytotoxicity, and oxidative stress. However, SS results in lung tumorigenesis, while CuNi fume does not. The reason for this divergence remains unclear. Cancer cells are dependent on Cu at greater levels than that of normal cells due to the increased metabolic demand. Therefore, limiting Cu in cancer cells has beneficial outcomes [10]. Conversely, excess Cu is cytotoxic and damaging to cancer cells [12, 45–47]. The mechanistic role of Cu in apoptosis, necroptosis, pyroptosis, ferroptosis, and cuproptosis, centered around mitochondrial dysfunction, has treatment options using repurposed drugs in combination to deliver increased Cu to cancer cells. In fact, Cu-based treatments decreased NNK-induced tumor number and size in agreement with the results of this study [13]. Our *in vitro* results of marked cytotoxicity and oxidative stress suggest a similar paradigm of increased delivery of Cu contributing to tumorigenesis prevention. This is supported by the *in vivo* results of a more pronounced effect of reduced tumor number with the HD CuNi exposure group compared to the LD, further illustrating that increased Cu delivery to the lung may be inhibitory to tumor promotion. Cumulatively, our results of various welding fumes suggest *in vivo* differences with fumes that are Fe-rich compared with those that are Cu-rich.

The potential role of Ni in the fume cannot be dismissed. A significant amount of literature exists on the role of Ni in welding fumes, and Ni is classified as carcinogenic to humans by IARC [48, 49]. Many studies have shown that Ni can damage DNA directly and through ROS production, epigenetic effects, and chromosomal aberrations [49, 50]. Numerous worker and *in vivo* studies have shown that exposure to Ni-containing SS welding fumes increases lung cancer risk [18, 21, 48, 49]. Because welding fume exposures do not represent pure exposure to Ni as seen with Ni-producing occupations, this elevated risk cannot be definitively linked to Ni or any other single metal component of the fume. Moreover, in 2012, IARC concluded that high cytotoxic concentrations and the presence of inflammation may be needed to see carcinogenic effects from Ni exposures [48]. Indeed, we showed that nickel oxide (NiO), as a surrogate metal component of SS welding fume, caused no lung cytotoxicity, lung inflammation, or tumor promotion [4]. These results suggest that the observed lung effects are generally due to the Cu component of this fume.

In conclusion, CuNi welding fume inhalation exposure decreased lung tumor size and lesion severity. The higher deposited dose decreased tumor multiplicity. This study highlights the need for ongoing research investigating CuNi welding fumes, especially in terms of delivered dose and dose rate. While the results of this study suggest less carcinogenicity of CuNi welding fume compared to Fe-rich fumes, additional studies are warranted to fully understand potential health outcomes.

Acknowledgments

The authors thank the NIOSH inhalation and animal quarters staff for their expert assistance with the animal inhalation exposures and the NIOSH histopathology core. Graphical abstract created with BioRender.com.

Author Contributions

P.C.Z-E., J.M.A., A.E. conceived and designed the experiments. P.C.Z.E., V.K., L.M.F., S.S.L., A.B.S., L.G., R.S., T.T-D., T.G.M., E.B., K.R.H., S.S., M.K., A.E., performed the experiments and did data analysis. L.A.B., R.M., W.M., S.S., S.F., provided technical support and critical comments. P.C.Z-E., L.M.F., A.E. drafted the manuscript. All authors participated in the revision of the manuscript and approved the submitted version.

Ethics Statement

All procedures were performed using protocols approved by the Centers for Disease Control Morgantown Institutional Animal Care and Use Committee.

Conflict of interest statement: None declared.

Funding

This work was supported by the National Institute for Occupational Safety and Health [927ZLEE and 9390DT2].

Disclaimer

The findings and conclusions in this report are those of the authors and do not necessarily represent the official position of the National Institute for Occupational Safety and Health, Centers for Disease Control and Prevention. Mention of a brand name does not constitute product endorsement.

Data Availability

Data will be made available via the National Institute for Occupational Safety and Health Gateway.

References

1. IARC. *Welding, Molybdenum Trioxide, and Indium Tin Oxide*. IARC Monographs on the Evaluation of Carcinogenic Risks to Humans, Vol. **118**. Lyon, France: IARC; 2018.
2. IARC. *Identification of Research Needs to Resolve the Carcinogenicity of High-Priority IARC Carcinogens*. IARC Technical Publication, No.**42**, Lyon, France: IARC; 2009, 40–9.
3. Falcone LM, Erdely A, Kodali V *et al*. Inhalation of iron-abundant gas metal arc-mild steel welding fume promotes lung tumors in mice. *Toxicology* 2018;**409**:24–32.
4. Falcone LM, Erdely A, Salmen R *et al*. Pulmonary toxicity and lung tumorigenic potential of surrogate metal oxides in gas metal arc welding–stainless steel fume: iron as a primary mediator versus chromium and nickel. *PLoS One* 2018;**13**:e0209413.
5. Zeidler-Erdely PC, Falcone LM, Antonini JM *et al*. Tumorigenic response in lung tumor susceptible A/J mice after sub-chronic exposure to calcium chromate or iron (III) oxide. *Toxicol Lett* 2020;**334**:60–5.
6. Antonini JM, Badding MA, Meighan TG *et al*. Evaluation of the pulmonary toxicity of a fume generated from a nickel- copper-based electrode to be used as a substitute in stainless steel welding. *Environ Health Insights* 2014;8:11–20.

7. Zeidler-Erdely PC, Erdely A, Kodali V *et al*. Lung toxicity profile of inhaled copper-nickel welding fume in A/J mice. *Inhal Toxicol* 2022;**34**:275–86.
8. Antonini JM. Health effects of welding. *Crit Rev Toxicol* 2003;**33**:61–103.
9. Copper Development Association Inc. *Joining Copper-Nickel Alloys*. 2024. https://www.copper.org (31 May 2024, date last accessed).
10. Tang X, Yan Z, Miao Y *et al*. Copper in cancer: from limiting nutrient to therapeutic target. *Front Oncol* 2023;**13**:1209156.
11. Lopez J, Ramchandani D, Vahdat L. Copper depletion as a therapeutic strategy in cancer. *Met Ions Life Sci* 2019;**19**:303–30.
12. Tsvetkov P, Coy S, Petrova B *et al*. Copper induces cell death by targeting lipoylated TCA cycle proteins. *Science* 2022;**375**:1254–61.
13. Bagherpoor AJ, Shameem M, Luo X *et al*. Inhibition of lung adenocarcinoma by combinations of sulfasalazine (SAS) and disulfiram-copper (DSF-Cu) in cell line models and mice. *Carcinogenesis* 2023;**44**:291–303.
14. Antonini JM, Afshari AA, Stone S *et al*. Design, construction, and characterization of a novel robotic welding fume generator and inhalation exposure system for laboratory animals. *J Occup Environ Hyg* 2006;**3**:194–203; quiz D45.
15. Fraser K, Kodali V, Yanamala N *et al*. Physicochemical characterization and genotoxicity of the broad class of carbon nanotubes and nanofibers used or produced in U.S. facilities. *Part Fibre Toxicol* 2020;**17**:62.
16. Organisation de coopération et de développement économiques. *Test No. 487: In vitro Mammalian Cell Micronucleus Test*. Paris, France: OECD Publishing, 2016.
17. Kodali V, Afshari A, Meighan T *et al*. *In vivo* and *in vitro* toxicity of a stainless-steel aerosol generated during thermal spray coating. *Arch Toxicol* 2022;**96**:3201–17.
18. Falcone LM, Erdely A, Meighan TG *et al*. Inhalation of gas metal arc-stainless steel welding fume promotes lung tumorigenesis in A/J mice. *Arch Toxicol* 2017;**91**:2953–62.
19. Shimkin MB, Stoner GD. Lung tumors in mice: application to carcinogenesis bioassay. *Adv Cancer Res* 1975;**21**:1–58.
20. Witschi HP, Williamson D, Lock S. Enhancement of urethan tumorigenesis in mouse lung by butylated hydroxytoluene. *J Natl Cancer Inst* 1977;**58**:301–5.
21. Zeidler-Erdely PC, Meighan TG, Erdely A *et al*. Lung tumor promotion by chromium-containing welding particulate matter in a mouse model. *Part Fibre Toxicol* 2013;**10**:45.
22. Renne R, Brix A, Harkema J *et al*. Proliferative and nonproliferative lesions of the rat and mouse respiratory tract. *Toxicol Pathol* 2009;**37**:5S–73S.
23. Cesta MF, Dixon D, Herbert RA, *et al*. *Respiratory System—Epithelium, Alveolus—Hyperplasia*. Research Triangle Park, NC, United States: National Toxicology Program Nonneoplastic Lesion Atlas, 2014.
24. Mann PC, Vahle J, Keenan CM *et al*. International harmonization of toxicologic pathology nomenclature: an overview and review of basic principles. *Toxicol Pathol* 2012;**40**:7S–13S.
25. McKinney W, Jackson M, Sager TM *et al*. Pulmonary and cardiovascular responses of rats to inhalation of a commercial antimicrobial spray containing titanium dioxide nanoparticles. *Inhal Toxicol* 2012;**24**:447–57.
26. Mercer RR, Scabilloni JF, Hubbs AF *et al*. Extrapulmonary transport of MWCNT following inhalation exposure. *Part Fibre Toxicol* 2013;**10**:38.
27. Ma J, Mercer RR, Barger M *et al*. Effects of amorphous silica coating on cerium oxide nanoparticles induced pulmonary responses. *Toxicol Appl Pharmacol* 2015;**288**:63–73.
28. Mercer RR, Scabilloni JF, Wang L *et al*. The fate of inhaled nanoparticles: detection and measurement by enhanced dark-field microscopy. *Toxicol Pathol* 2018;**46**:28–46.
29. Erdely A, Hulderman T, Salmen-Muniz R *et al*. Inhalation exposure of gas-metal arc stainless steel welding fume increased atherosclerotic lesions in apolipoprotein E knockout mice. *Toxicol Lett* 2011;**204**:12–6.
30. Groch KM, Khan MA, Brooks AL *et al*. Lung cancer response following inhaled radon in the A/J and C57BL/6J mouse. *Int J Radiat Biol* 1997;**71**:301–8.
31. Curtin GM, Higuchi MA, Ayres PH *et al*. Lung tumorigenicity in A/J and rasH2 transgenic mice following mainstream tobacco smoke inhalation. *Toxicol Sci* 2004;**81**:26–34.
32. Antonini JM, Stone S, Roberts JR *et al*. Effect of short-term stainless steel welding fume inhalation exposure on lung inflammation, injury, and defense responses in rats. *Toxicol Appl Pharmacol* 2007;**223**:234–45.
33. Antonini JM, Roberts JR, Stone S *et al*. Short-term inhalation exposure to mild steel welding fume had no effect on lung inflammation and injury but did alter defense responses to bacteria in rats. *Inhal Toxicol* 2009;**21**:182–92.
34. Zeidler-Erdely PC, Battelli LA, Stone S *et al*. Short-term inhalation of stainless steel welding fume causes sustained lung toxicity but no tumorigenesis in lung tumor susceptible A/J mice. *Inhal Toxicol* 2011;**23**:112–20.
35. Badding MA, Fix NR, Antonini JM *et al*. A comparison of cytotoxicity and oxidative stress from welding fumes generated with a new nickel-, copper-based consumable versus mild and stainless steel-based welding in RAW 264.7 mouse macrophages. *PLoS One* 2014;**9**:e101310.
36. Ahamed M, Akhtar MJ, Alhadlaq HA *et al*. Assessment of the lung toxicity of copper oxide nanoparticles: current status. *Nanomedicine (Lond)* 2015;**10**:2365–77.
37. Akhtar MJ, Kumar S, Alhadlaq HA *et al*. Dose-dependent genotoxicity of copper oxide nanoparticles stimulated by reactive oxygen species in human lung epithelial cells. *Toxicol Ind Health* 2016;**32**:809–21.
38. Strauch BM, Niemand RK, Winkelbeiner NL *et al*. Comparison between micro- and nanosized copper oxide and water soluble copper chloride: interrelationship between intracellular copper concentrations, oxidative stress and DNA damage response in human lung cells. *Part Fibre Toxicol* 2017;**14**:28.
39. Siivola KM, Suhonen S, Hartikainen M *et al*. Genotoxicity and cellular uptake of nanosized and fine copper oxide particles in human bronchial epithelial cells *in vitro*. *Mutat Res Genet Toxicol Environ Mutagen* 2020;**856–857**:503217.
40. Kim JS, Adamcakova-Dodd A, O'Shaughnessy PT *et al*. Effects of copper nanoparticle exposure on host defense in a murine pulmonary infection model. *Part Fibre Toxicol* 2011;**8**:1–14.
41. Gosens I, Cassee FR, Zanella M *et al*. Organ burden and pulmonary toxicity of nano-sized copper (II) oxide particles after short-term inhalation exposure. *Nanotoxicology* 2016;**10**:1084–95.
42. Poland C, Hubbard SA, Levy L *et al*. Inhalation toxicity of copper compounds: results of 14-day range finding study for copper sulphate pentahydrate and dicopper oxide and 28-day subacute inhalation exposure of dicopper oxide in rats. *Toxicology* 2022;**474**:153221.
43. Haase L-M, Birk T, Poland CA *et al*. Cross-sectional study of workers employed at a copper smelter-effects of long-term exposures to copper on lung function and chronic inflammation. *J Occup Environ Med* 2022;**64**:e550–8.
44. Stratmann H, Wohlleben W, Wiemann M *et al*. Classes of organic pigments meet tentative PSLT criteria and lack toxicity in short-term inhalation studies. *Regul Toxicol Pharmacol* 2021;**124**:104988.
45. Gupte A, Mumper RJ. Elevated copper and oxidative stress in cancer cells as a target for cancer treatment. *Cancer Treat Rev* 2009;**35**:32–46.
46. Macomber L, Imlay JA. The iron-sulfur clusters of dehydratases are primary intracellular targets of copper toxicity. *Proc Natl Acad Sci USA* 2009;**106**:8344–9.
47. Jiang Y, Huo Z, Qi X *et al*. Copper-induced tumor cell death mechanisms and antitumor theragnostic applications

of copper complexes. *Nanomedicine (Lond)* 2022;**17**: 303–24.
48. *Chromium, Nickel and Welding, IARC Monographs on the Evaluation of Carcinogenic Risks to Humans*, Vol. **49**. Lyon, France: IARC; 1990, 1–648.
49. *Arsenic, Metals, Fibres, and Dusts*. IARC Monographs on the Evaluation of Carcinogenic Risks to Humans, Vol. **100**. Lyon, France: IARC; 2012, 11–465.
50. Kasprzak KS, Sunderman FW, Salnikow K. Nickel carcinogenesis. *Mutat Res* 2003;**533**:67–97.